Carrier-Based PWM Overmodulation Strategies for Five-Phase Inverters

(Article begins on next page)

21 December 2024

Carrier-Based PWM Overmodulation Strategies for Five-Phase Inverters

L. Vancini, M. Mengoni, *Member, IEEE*, G. Rizzoli, G. Sala, *Member, IEEE,*
L. Zarri, *Senior Member, IEEE,* and A. Tani

Abstract – In three-phase electric drives, overmodulation is commonly used to fully exploit the dc-bus voltage, increase the dynamic performance of the motor, and reduce the inverter switching frequency. The same advantages can be found in multiphase converters, where a higher number of degrees of freedom allows defining new operating modes. In this paper, the extension of the overmodulation strategies of three-phase inverters to five-phase systems is investigated. Experimental tests on a five-phase induction motor drive are carried out to verify the feasibility of the developed techniques, the quality of the current waveforms, and the improvement in the dynamic performance of the drive.

I. INTRODUCTION

Multiphase drives play a crucial role in high-reliability applications where fault tolerance is an essential requirement to guarantee the operation in critical conditions. The marine and aeronautical applications well represent this combination of robustness requirements and high-power operating conditions [1]-[4]. Furthermore, multiphase systems have features that make them competitive in many other industrial areas. An increase in the number of phases of an electric machine permits improving the torque density [5], reducing the noise levels [6]-[7], and developing multi-motor applications [8]-[9].

A multiphase motor drive is usually fed by a multiphase inverter, which is the generalization of a three-phase inverter obtained through the parallel connection of a higher number of inverter legs. In three-phase systems, the most widespread control techniques are the carrier-based Pulse Width Modulation (PWM) and the Space Vector Modulation (SVM). The same strategies can be extended to multiphase converters. The analysis is difficult because the high number of inverter configurations cannot be described through a two-dimensional representation but requires a multidimensional description. The Vector Space Decomposition (VSD) solves this problem by introducing new complex planes or subspaces that are intrinsically linked to specific spatial harmonics of the magnetic field of an electric machine [10].

The approach based on multiple space vectors also allows calculating of the voltage limits of the converter. A simplified explicit relationship linking the magnitudes of the voltage vectors is available for multiphase inverters with an odd number of phases [11]. Implicitly, this solution defines the

For this reason, different strategies have been developed to approximate the reference voltage space vector or to improve the performance of the motor drive [12]-[14].

This paper aims to extend some of the most consolidated overmodulation methods for three-phase inverters to five-phase inverters (Fig. 1). Some literature already exists on this topic. A specific solution is presented in [15] for a dual three-phase permanent-magnet synchronous motor drive, while a solution for an odd generic number of phases is proposed in [16]. The approach in [16] is based on an efficient iterative technique proposed by James A. Cadzow to find the minimum infinity-norm solution of an under-determined linear system. The solutions in [17] –[19] use the SVM approach for five phase inverters, while the one in [20] is valid for a generic number of phases. Finally, the same authors of [16] applied their method to five-phase inverters in [21].

The overmodulation strategies distort the output voltage in multiphase systems as well as in three-phase systems. An output filter can be a viable tool to reduce the harmonics of the output current and enhance the exploitation of the dc-bus [22].

In the present paper, a thorough analysis of the overmodulation for five-phase inverters is presented. It shows that the voltage domain of multiphase converters includes two overmodulation regions (Fig. 2). The first one, which is here called *extended linear region*, has not a counterpart in three-phase inverters. It is defined as the operating conditions where the converter can generate the reference voltage vector in the fundamental subspace, but the voltage vectors in the other subspaces cannot be zero.

The second operating area is the so-called *overmodulation region*, where the match between the reference voltage and the actual voltage can be only approximative, even in the fundamental subspace. On the one hand, the converter generates voltage harmonic components at low frequency, which deteriorate the quality of the phase currents and cause additional losses in the motor. On the other hand, the overmodulation operation reduces the number of switch commutations and the inverter switching losses.

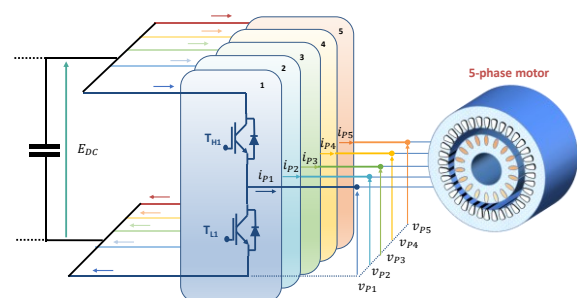Also, an algorithm for the modulation in the extended

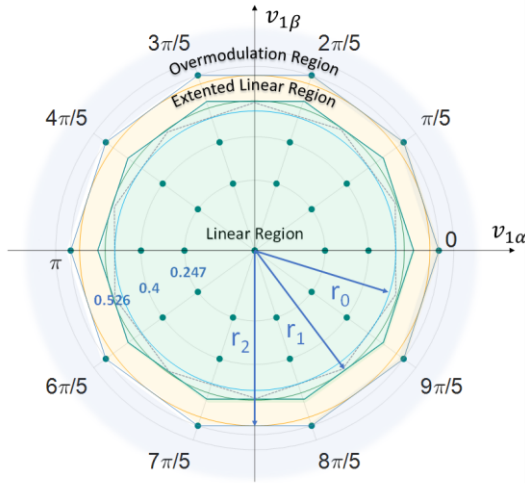Fig. 1 – Schematics of a five-phase motor drive.

Fig. 2 – Modulation regions in a five-phase inverter.

linear region of five-phase inverters is presented. Compared to the previous solutions, this algorithm generates the lowest voltage distortion and does not require iterations to converge.

Overall, the main contributions of this paper are as follows:

i) Clear distinction between the concepts of extended linear modulation and overmodulation

ii) Rigorous development of a modulation strategy with the minimum voltage distortion in the extended linear region, which does not require iterative calculations

iii) Further extension of the modulation range by adapting the most common overmodulation techniques for three-phase inverters to five-phase systems

iv) Experimental comparison of the overmodulation strategies.

This paper is organized as follows. Section II illustrates the overmodulation operation of five-phase inverters. This part includes the problem formulation for multiphase systems, the boundaries of the linear modulation, and a solution to minimize the voltage distortion. In Section III, the experimental results obtained with a five-phase induction motor drive are presented. The tests describe the dynamic performance, the harmonic distortion, and the average switching frequency for four different overmodulation strategies.

II. Modulation Regions in Five Phase Inverters

The analysis of five-phase systems is usually based on the definitions of space vectors and zero-sequence component. For a given set of real variables $x_1, ..., x_5$, a new set of variables $x_0, \bar{x}_1$ and $\bar{x}_3$ can be defined through the following symmetrical linear transformations:

$$x_0 = \frac{1}{5} \sum_{k=1}^{5} x_k \qquad (1)$$

$$\bar{x}_\rho = \frac{2}{5} \sum_{k=1}^{5} x_k \bar{\alpha}_k^\rho \qquad \rho = 1, 3 \qquad (2)$$

where

$$\bar{\alpha}_k = e^{j\frac{2}{5}\pi(k-1)}. \qquad (3)$$

The real quantity x_0 defined in (1) is the zero-sequence

component, whereas $\bar{x}_\rho$ (ρ = 1, 3), usually called "multiple space vectors," are complex quantities. Transformations (1)-(2) can be applied to the modulating signals m_k (k=1, ..., 5) of the inverter legs of a five-phase inverter to define the zero-sequence component m_0 and the multiple space vectors $\bar{m}_1$ and $\bar{m}_3$. The inverse transformation is as follows:

$$m_k = m_0 + \bar{m}_1 \cdot \bar{\alpha}_k + \bar{m}_3 \cdot \bar{\alpha}_k^3 \qquad (4)$$

where the dot operator "·" is defined as the real part of the product of the first operand and the complex conjugate of the second operand. The link between the modulating signals and the phase voltages is through the following equations:

$$m_0 = \frac{v_0}{E_{DC}} \qquad (5)$$

$$\bar{m}_\rho = \frac{\bar{v}_\rho}{E_{DC}} \qquad \rho = 1, 3 \qquad (6)$$

where E_{DC} is the dc-link voltage, $\bar{v}_1, \bar{v}_3$ are the voltage vectors and v_0 is the desired zero-sequence component of the inverter pole voltages (sometimes called common-mode voltage).

The modulating signals must satisfy the following constraints:

$$m_k \in [0,1] \quad k=1, ..., 5. \qquad (7)$$

Generally, the reference value for $\bar{v}_1$ is generated by the motor control system (Fig. 3), whereas m_0 in (4) is a degree of freedom. For example, Sinusoidal PWM (SPWM) keeps m_0 equal to 0.5 over a switching period. Under the assumption of sinusoidal phase voltages, SPWM allows the voltage vector $\bar{v}_1$ to reach a magnitude of $0.5E_{DC}$. Its linear range is graphically represented in Fig. 2 by the circle with a normalized radius r_0 of 0.5. However, other values of m_0 can be used to maximize the voltage range [23], to optimize some characteristics of the converter, such as the switching losses [24], the spectrum of the output current [25], [26], the sizing of the dc-link capacitors, and the common-mode current [27]. Conversely, $\bar{v}_3$ can be chosen in order to reduce the harmonic distortion of the stator current [28], perform an encoder-less control [29], ensure fault tolerance [30], estimate the motor parameters [31], and implement a multi-motor drive [9].

In this paper, $\bar{v}_3$ is used to extend the linear modulation region of $\bar{v}_1$. Inequalities (7) generate some complicated constraints on the admissible values of $\bar{m}_1$ and $\bar{m}_3$ in each switching period. If $\bar{m}_3$ is set to zero, and the phase angle of $\bar{m}_1$ is not considered, the problem of the modulation range has a simple solution, corresponding to circle with radius r_1 in Fig. 2 [11].

$$|\bar{m}_{1,ref}| \leq \frac{1}{2 \cos\left(\frac{\pi}{10}\right)} \approx 0,526. \qquad (8)$$
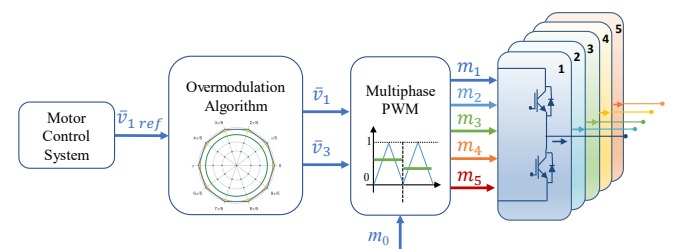

Fig. 3 – Schematics of the control system for a five-phase inverter.

The constraints in (7) imply the following equivalent set of inequalities:

$$m_k - m_i \leq 1 \quad k = 1, ..., 5; \ i = 1, ..., 5 \quad (9)$$

These inequalities should be verified for each value of k and i and assert that the maximum distance among the modulating signals must not exceed 1. For the continuation of the analysis, it is useful to sort the signals m_k (k=1, 2, …, 5) in ascending order. Let L, D, M, U, H (from the initials of the words *low*, *down*, *medium*, *up*, *high*) be the indexes of the ordered modulating signals so that

$$m_L \leq m_D \leq m_M \leq m_U \leq m_H. \quad (10)$$

By using this notation, it is straightforward to prove that (9) is equivalent to (11):

$$m_H - m_L \leq 1. \quad (11)$$

In other words, a converter operates in the linear modulation region if the difference between the highest (Hth) and lowest (Lth) modulating signal is lower than one.

The necessary and sufficient condition (11) for linear modulation can be rewritten by means of (4) in the following form:

$$\bar{m}_1 \cdot (\bar{\alpha}_H - \bar{\alpha}_L) + \bar{m}_3 \cdot (\bar{\alpha}_H^3 - \bar{\alpha}_L^3) \leq 1. \quad (12)$$

The common-mode signal m_0 is not present in (12), so this variable does not affect the range of the linear modulation of the converter. Conversely, $\bar{m}_3$ can be selected to extend the boundaries of the admissible domain of $\bar{m}_1$. Among the possible values of $\bar{m}_3$ that improve the range of $\bar{m}_1$, the one with the minimum magnitude of $\bar{m}_3$ leads to the lowest rms value of the voltage distortion.

A performance index that can be used to assess the extension of the voltage range is the maximum modulation index MI in balanced and symmetric sinusoidal operating conditions, defined as the ratio of the magnitude of the voltage $\bar{v}_1$ and the dc-link voltage E_{DC}:

$$MI = \frac{|\bar{v}_1|}{E_{DC}}. \quad (13)$$

This index is used in the next section to compare different overmodulation strategies with one another.

A. Linear Modulation Region

Fig. 3 shows a conceptual block diagram for the generation of the output voltages in a five-phase inverter. The control system of the motor calculates the reference voltage $\bar{v}_{1\,ref}$ and sets the value of $\bar{v}_{3\,ref}$ to zero because it assumes that the converter operates in the linear region. The anti-transformation (4) allows calculating the modulating signals m_k with an arbitrary choice of the zero-sequence component m_0.

As shown in (12), if $\bar{m}_3$ is zero, the boundary of the linear modulation region for $\bar{m}_{1,ref}$ satisfies the following inequality:

$$\bar{m}_{1,ref} \cdot (\bar{\alpha}_H - \bar{\alpha}_L) \leq 1. \quad (14)$$

The admissible domain of $\bar{m}_{1,ref}$ is a regular decagon circumscribing the circle with radius $r_1 = 0.526$ in Fig. 2.

When (14) cannot be satisfied due to the amplitude of $\bar{m}_{1,ref}$, a suitable value of $\bar{m}_3$ can be used to satisfy (12) and preserve the reference vector $\bar{m}_{1,ref}$.

B. Extended Linear Modulation Region

In three phase inverters, a voltage vector, plotted in the complex plane, belongs only to the linear modulation region and the overmodulation region. In contrast, in multiphase inverters, there is an additional region, the extended linear modulation region (Fig. 2), where the vector $\bar{v}_{1,ref}$ can be synthesized without harmonic distortion if an appropriate vector $\bar{v}_3$ is used to satisfy (12). In other words, the voltage reference $\bar{v}_{1,ref}$ can be tracked, but $\bar{v}_3$ cannot be zero anymore.

In general, for a given value of $\bar{m}_{1,ref}$, several values of $\bar{m}_{3,ref}$ satisfy (13). In this paper, the desired solution is the one with the lowest amplitude of $\bar{m}_3$ so that the resulting voltage distortion, proportional to $|\bar{m}_3|$, is the lowest. For this purpose, (12) should be rewritten as follows:

$$\bar{m}_3 \cdot \bar{A}_{3,H,L} \leq 1 - \bar{m}_1 \cdot \bar{A}_{1,H,L} \quad (15)$$

where

$$\bar{A}_{1,H,L} = \bar{\alpha}_H - \bar{\alpha}_L \quad (16)$$
$$\bar{A}_{3,H,L} = \bar{\alpha}_H^3 - \bar{\alpha}_L^3. \quad (17)$$

The value of $\bar{m}_3$ can be decomposed along two orthogonal directions, respectively parallel and orthogonal to $\bar{A}_{3,H,L}$:

$$\bar{m}_3 = \bar{A}_{3,H,L}(\lambda + j\mu) \quad (18)$$

where λ and μ are the degrees of freedom of $\bar{m}_3$. The magnitude of $\bar{m}_3$ can be expressed as follows:

$$|\bar{m}_3| = |\bar{A}_{3,H,L}|\sqrt{\lambda^2 + \mu^2}. \quad (19)$$

The admissible values of λ can be calculated by substituting (18) in (15). It follows:

$$\lambda \leq \frac{1 - \bar{m}_{1,ref} \cdot \bar{A}_{1,H,L}}{\left|\bar{A}_{3,H,L}\right|^2}. \quad (20)$$

According to (14), the numerator of (20) is negative outside the linear modulation region, while the denominator is indeed positive. Therefore, the value of λ that minimizes the amplitude of $\bar{m}_3$ in (19) is the upper bound of (20):

$$\lambda = \frac{1 - \bar{m}_{1,ref} \cdot \bar{A}_{1,H,L}}{\left|\bar{A}_{3,H,L}\right|^2}. \quad (21)$$

To determine the value of μ, it is necessary to verify that $\bar{m}_3$ does not alter the order of the modulating signals assumed in (10), namely H is the index of the highest modulating signal, and L is the index of the lowest modulating signal. In practice, it is sufficient to verify that m_H is higher than the neighboring value m_U, and m_L is lower than the neighboring value m_D.

$$\begin{cases} m_H \geq m_U \\ m_L \leq m_D \end{cases}. \quad (22)$$

Substituting (4), (18) and (21) in (22) leads to the following inequalities:

$$\begin{cases} \mu(j\bar{A}_{3,H,L} \cdot \bar{A}_{3,H,U}) \geq -\bar{m}_{1,ref} \cdot \bar{A}_{1,H,U} - \lambda(\bar{A}_{3,H,L} \cdot \bar{A}_{3,H,U}) \\ \mu(j\bar{A}_{3,H,L} \cdot \bar{A}_{3,L,D}) \leq -\bar{m}_{1,ref} \cdot \bar{A}_{1,L,D} - \lambda(\bar{A}_{3,H,L} \cdot \bar{A}_{3,L,D}) \end{cases}. \quad (23)$$

The system of linear inequalities (23) identifies a range of

values for μ. Let μ_{max} and μ_{min} be respectively the upper and lower ends:

$$\mu_{min} \leq \mu \leq \mu_{max}. \tag{24}$$

If μ_{max} is positive and μ_{min} is negative, choosing μ equal to zero minimizes the amplitude of $\bar{m}_3$. Conversely, if μ_{max} and μ_{min} are both positive (or negative), μ must be chosen equal to the lowest absolute value between them.

$$\begin{cases} if\, \mu_{max}\, \mu_{min} \leq 0 \Rightarrow \mu = 0 \\ if\, \mu_{max}\, \mu_{min} > 0 \Rightarrow \mu = \begin{cases} \mu_{max}\ if\ |\mu_{max}| < |\mu_{min}| \\ \mu_{min}\ if\ |\mu_{min}| < |\mu_{max}| \end{cases} \end{cases} \tag{25}$$

When $\bar{v}_{1,ref}$ is on the boundary of the extended linear region, the interval $[\mu_{min}, \mu_{max}]$ collapses into a single point, and the solution of (23) is unique. This operating condition is remarkable as it corresponds to the situation in which the two highest modulating signals m_H and m_U are both equal to 1, and the two lowest modulating signals m_L and m_D are zero [22].

$$\begin{cases} m_H = m_U \\ m_L = m_D \end{cases}. \tag{26}$$

Replacing (4) in (26), one obtains:

$$\begin{cases} \bar{m}_{3,ref} \cdot \bar{A}_{3,H,U} = -\bar{m}_{1,ref} \cdot \bar{A}_{1,H,U} \\ \bar{m}_{3,ref} \cdot \bar{A}_{3,L,D} = -\bar{m}_{1,ref} \cdot \bar{A}_{1,L,D} \end{cases} \tag{27}$$

The unique solution of (27) is

$$\bar{m}_{3,ref} = j\frac{(\bar{m}_{1,ref} \cdot \bar{A}_{1,H,U})\bar{A}_{3,L,D} - (\bar{m}_{1,ref} \cdot \bar{A}_{1,L,D})\bar{A}_{3,H,U}}{(j\bar{A}_{3,H,U}) \cdot \bar{A}_{3,L,D}}. \tag{28}$$

The value of $\bar{m}_3$ given by (28) allows $\bar{m}_{1,ref}$ to reach the boundary of the decagon depicted in Fig. 2, whose inscribed circle has a radius equal to:

$$r_2 = \frac{2}{5}\left[1 + 2cos\left(\frac{2}{5}\pi\right)\right]cos\left(\frac{\pi}{10}\right) \approx 0.616. \tag{29}$$

Above this value, the converter operates in the overmodulation region, which is analyzed in the next Section.

The main equations of the linear and extended linear regions are reported in Table I.

C. Overmodulation Region

In the overmodulation region, it is not possible to supply

the load with the requested voltage vector, but only with a fraction of it. The technique explained in Section II.B finds a suitable value of $\bar{m}_{3,ref}$ to reach the frontier of the overmodulation region. In these operating condition, the voltage reference $\bar{m}_{3,ref}$ is equal to (28), as this value allows maximizing the amplitude of $\bar{m}_{1,ref}$. However, beyond this operating point, the reference space vectors $\bar{m}_{1,ref}$ cannot be generated whatever the value of $\bar{m}_{3,ref}$.

In overmodulation conditions, the generated vectors $\bar{m}_1$ and $\bar{m}_3$ are different from the reference vectors $\bar{m}_{1,ref}$ and $\bar{m}_{3,ref}$. In particular, $\bar{m}_1$ cannot cover a circular path at steady state. Since $\bar{m}_1$ controls the current vector in the fundamental subspace, which is in turn related to the magnetic field in the air gap, a certain level of torque ripple is unavoidable.

Three well-consolidated overmodulation methods for three-phase inverters are the Minimum Distance (MD), the Minimum Phase Error (MPE) and Bolognani's modulation (Bs) [12], [32], [33]. These techniques can be easily generalized to multiphase systems operating in the overmodulation region, as shown in Fig. 4. The performance of the multiphase overmodulation strategies is shown in Fig. 5 and briefly explained hereafter.

The MPE overmodulation method consists in dividing the modulating signal $m_{k,ref}$ of each inverter leg by a normalization factor, which does not affect either the phase angles of the space vectors $\bar{v}_1$ and $\bar{v}_3$ or the ratio of their magnitudes, but only the respective amplitudes, so that the modulating signals fit the interval [0,1]:

$$m_k = \frac{m_{k,ref} - m_{L,ref}}{m_{H,ref} - m_{L,ref}} \qquad k = 1,...,5. \tag{30}$$

It can be verified that this solution leads to a reduction in the harmonic distortion of the phase currents compared to the
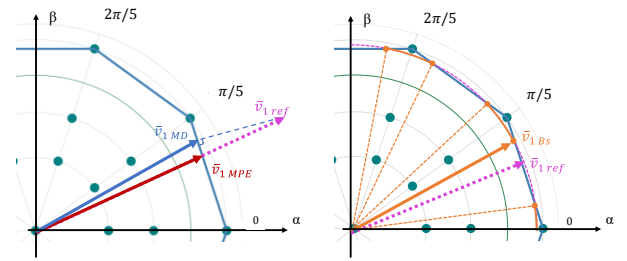
Fig. 4 – Generation of the output voltage vector starting from the reference voltage $\bar{v}_{1\,ref}$ according to the minimum phase error strategy $(\bar{v}_{1\,MPE})$, minimum distance strategy $(\bar{v}_{1\,MD})$ and multiphase Bolognani's overmodulation $(\bar{v}_{1\,Bs})$.
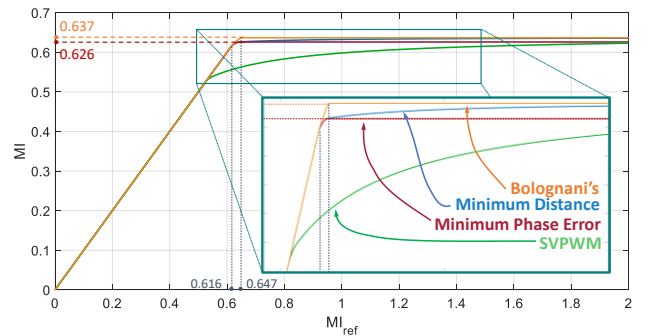
Fig. 5 – Requested modulation index MI_{ref} versus modulation index MI.

TABLE I
SPACE VECTORS OF THE MODULATING SIGNALS
IN DIFFERENT MODULATION REGIONS

Modulation Region	$\bar{m}_1, \bar{m}_3$
Linear Modulation	$\bar{m}_{1\,ref} = \bar{m}_1,\ \bar{m}_{3\,ref} = 0$
Extended Linear Modulation	$\bar{m}_{1\,ref} = \bar{m}_1,\ \bar{m}_{3\,ref} = \bar{A}_{3,H,L}(\lambda + j\mu)$ $\lambda = \dfrac{1 - \bar{m}_1 \cdot \bar{A}_{1HL}}{\lvert\bar{A}_{3,H,L}\rvert^2}$ $if\,\mu_{max}\,\mu_{min} \leq 0,\ \mu = 0$ $if\,\mu_{max}\,\mu_{min} > 0,\ \mu = \begin{cases} \mu_{max}\ if\ \lvert\mu_{max}\rvert < \lvert\mu_{min}\rvert \\ \mu_{min}\ if\ \lvert\mu_{min}\rvert < \lvert\mu_{max}\rvert \end{cases}$
Overmodulation	$\bar{m}_{1\,ref} \neq \bar{m}_1,$ $\bar{m}_{3\,ref} = j\dfrac{(\bar{m}_{1,ref} \cdot \bar{A}_{1,H,U})\bar{A}_{3,L,D} - (\bar{m}_{1,ref} \cdot \bar{A}_{1,L,D})\bar{A}_{3,H,U}}{(j\bar{A}_{3,H,U}) \cdot \bar{A}_{3,L,D}}$

other considered techniques, while the maximum modulation index becomes

$$MI_{MPE\,max} \approx 0.626. \tag{31}$$

As with three-phase inverters, the multiphase MPE technique does not lead to a pure square wave operation even at a very high modulation index.

The MD overmodulation minimizes the error between the requested voltage vector and the voltage vector generated by the inverter (in the fundamental subspace). Remarkably, the modulating signals can be calculated easily even for a five-phase inverter. Initially, it is necessary to calculate the zero-sequence component m_0 of the desired voltage vector with the following expression:

$$m_0 = \frac{(1 - n_H - n_L)}{2} \tag{32}$$

where H and L are the indexes already defined in (10) and

$$n_k = \bar{m}_{1,ref} \cdot \bar{\alpha}_k + \bar{m}_{3,ref} \cdot \bar{\alpha}_k^3 \qquad k = 1, ..., 5 \tag{33}$$

and $\bar{m}_{3,ref}$ is given by (28).

Then, the kth modulating signal ($k=1, ..., 5$) is calculated as usual as:

$$m_k = m_0 + n_k \tag{34}$$

and is clamped in the range [0,1]. In the overmodulation region, the two highest modulating signals are equal to 1, while the two lowest modulating signals are equal to 0. An insightful proof that this procedure leads to the lowest magnitude error of $\bar{v}_{1,ref}$ is reported in Appendix A.

The largest modulation index obtainable by the MD strategy is slightly greater than the one obtainable by the MPE technique. The output pole voltages tend to a square-wave waveform only if the magnitude of $\bar{v}_{1,ref}$ tends to infinite (Fig. 5).

$$MI_{MD\,max} = \frac{2}{\pi} \approx 0.637 \tag{35}$$

Bolognani's modulation Bs was introduced for the first time for three-phase systems in [33]. In its multiphase counterpart, the output voltage vector in the overmodulation region is the one with the lowest phase error among the admissible vectors with the lowest magnitude error. In practice, whenever the requested voltage exceeds the extended linear region, represented by the decagon of Figs. 2 and 4, the output voltage is kept equal to the value that it has in the crossing point, as shown in Fig. 4(b). If the requested voltage increases further, the inverters quickly tends to the square-wave operation that uses only the ten vectors placed on the vertices of the decagon. Among all the presented techniques, this is the only one that allows obtaining a square wave operation with a finite modulation index (MI=0.647).

In Fig. 5, MD, MDE and Bs overmodulation strategies are compared with each other and with the traditional Space Vector Pulse Width Modulation (SVPWM). Although SVPWM can be implemented as an SVM strategy, namely the one that uses two zero vectors, equally allocated in the middle and at the end of the switching pattern, in this paper, it is considered as a carrier-based center-aligned pulse-width modulation technique whose zero-sequence component is given by (32) with $\bar{v}_{3,ref}$ equal to zero [34]. If some of the resulting duty-cycles are outside the range [0,1], they are clipped to the interval edges.

In the graph of Fig. 5, the desired modulation index MI_{ref} is shown on the horizontal axis, while the actual modulation index MI is shown on the vertical axis.

When the modulation index exceeds r_1 (0.526), the SVPWM technique maintains $\bar{v}_3$ equal to zero, thus causing a non-linear relationship between $\bar{v}_{1,ref}$ and the actual voltage $\bar{v}_1$. Conversely, by choosing a suitable value of the vector $\bar{v}_3$, it is possible to keep $\bar{v}_1$ equal to the desired one, $\bar{v}_{1,ref}$ in the extended linear region.

When MI_{ref} exceeds r_2 (0.616), the MD, MPE and Bs overmodulation strategies have slightly different behaviors. While Bs strategy quickly converges to a square-wave operation, the convergence rate of MD strategy is slower. In contrast, MPE strategy never reaches the pure square-wave operation and the maximum modulation index is slightly lower. The SVPWM strategy has the same performance as the MPE strategy but only for very high values of the modulation index (above 2.5).

In conclusion, the highest voltage cannot be used as an indicator to compare the performance of the overmodulation algorithms with one another. Conversely, the linearity error of the modulation process, i.e., the difference between the desired voltage and the actual voltage, and the voltage quality appear to be particularly relevant because they can significantly affect the transient and steady-state response of an electric drive.

D. Calculation of m_0

In general, m_0 can be chosen according to different rules. Since the duty-cycles must belong to the range [0,1], it is straightforward to derive the following inequality from (34):

$$-n_L \leq m_0 \leq 1 - n_H. \tag{36}$$

Any value of m_0 that satisfies (36) can be used for the calculation of the modulating signals. Typically, discontinuous modulations favor the ends of the range (36), whereas SVPWM uses the mid-point (32).

If the desired voltage vector $\bar{v}_{1,ref}$ belongs to the linear region or extended linear region, many interchangeable choices are theoretically possible for m_0. Conversely, in the overmodulation operation, the range of m_0 collapses into a single value, and the upper bound of (36) becomes equal to the lower bound. Even in this case, the value of m_0 can be calculated through (32).

Finally, it is worth noting that the meaning of m_0 is profoundly different from the one of $\bar{m}_3$. In multiphase inverters, $\bar{m}_1$ and $\bar{m}_3$ are usually considered as set-point vectors given by the control system, and m_0 is a degree of freedom. However, in this paper, only $\bar{m}_1$ is a set-point vector, whereas m_0 and $\bar{m}_3$ are degrees of freedom. The presence of $\bar{m}_3$ as a new optimizable complex variable allows extending the linear modulation range of $\bar{m}_1$ despite the generation of low-frequency voltage harmonics in subspace α_3-β_3, which can also be seen in the line-to-line voltages. As a result, changing $\bar{m}_3$ is quite different from changing m_0, which never affects the line-to-line voltages.

E.   Usage Constraints and Final Remarks

The overmodulation strategies presented in this paper should be used for machines that have a sinusoidal back-emf and a significant value of the stator inductance. The VSD allows splitting the equations of a five-phase machine into two independent vector spaces, namely subspaces α_1-β_1 and α_3-β_3. Depending on the machine design, the air-gap magnetic field can contain a spatial harmonic, such as the third one, which may lead to an undesired electromotive force (emf) in subspace α_3-β_3 while the field wave is rotating. To prevent the circulation of an uncontrolled current in this subspace, the control system must compensate for the induced emf and applies a stator voltage $\bar{v}_3$ that counterbalances it. Conversely, if the air-gap field is sinusoidal, the electromotive force in subspace α_3-β_3 is negligible. The control system does not have to compensate for it, and it can use $\bar{v}_3$ for other purposes, such as extending the voltage range. However, since $\bar{v}_3$ is chosen for a purpose other than current control, a distorted current may circulate in the stator winding. Unlike the previous case, this drawback is the result of a voluntary action of the control system and is limited to the extended-linear and overmodulation operation. Also, it can be mitigated by the filtering action of the phase inductance. This latter consideration implies that the quality of the current in the overmodulation region is better in machines with a high stator inductance. An analysis of the current distortion when the inverter does not operate in the linear region is not straightforward. The equation of the current in subspace α_3-β_3 depends on the type of the motor (induction or synchronous machine), the winding design (sinusoidally-distributed winding or concentrated winding), other machine parameters such as the motor resistances, and the motor speed. In multiphase SPM synchronous machines, the distortion of the stator current in subspace α_3-β_3 is attenuated by a low-pass filter roughly composed of the stator resistance R_S and the synchronous inductance L_{S3} of that subspace. In induction machines, the filter has a more complex structure because it involves the stator and the rotor parameters.

The design of special filters could be a viable solution to mitigate the problems of the current harmonics in overmodulation and increase the exploitation of the dc-bus voltage [22].

III.   Experimental Results

A.   Experimental setup

The experimental setup used to verify the effectiveness of the modulation strategies consists of a five-phase wound-rotor induction motor, and a five-phase IGBT inverter. A picture of the experimental set-up is shown in Fig. 6.

The motor is a 30-slots five-phase induction machine with three pairs of poles and distributed windings.

The parameters of the machine, experimentally determined, are listed in Table II, whereas those of the inverter are shown in Table III.

The tests at steady state, such as the measurements of the voltage loci and current THD, have been carried out by using the inverter as a voltage source with an open-loop control. Conversely, a vector control scheme has been used in the

TABLE II
PARAMETERS OF THE FIVE-PHASE MACHINE

$\omega_{m,rated} = 15.7$ rad/s	(150 rpm)	$p = 3$
$L_{S1} = 411$ mH	$L_{S3} = 68$ mH	$M_1 = 555$ mH
$L_{R1} = 939$ mH	$L_{R3} = 158$ mH	$M_3 = 53$ mH
$R_S = 1.7$ Ω	$R_{R1} = 4.8$ Ω	$R_{R3} = 4.8$ Ω

TABLE III
PARAMETERS OF THE INVERTER

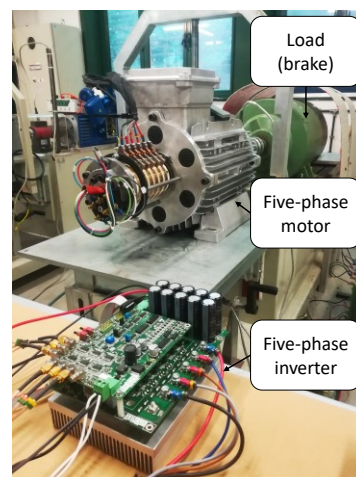| IGBT I_{max}=10 A, E_{DC}=100 V |
|---|
| Switching frequency 5 kHz, Dead Time 1.6 µs |
| DC-link capacitance 1100 µF |

Fig. 6. Experimental set-up of the electric drive composed by a five-phase wound-rotor induction machine and a five-phase inverter.

transient tests. It is based on a rotor flux-oriented control scheme for induction motors, and its block diagram is shown in Fig. 7. PI controller (a) adjusts the reference value for the torque-producing component of the stator current, depending on the actual speed error. Two PI controllers, (b) and (c), track the current references of the components of the stator current in the d_1-q_1 reference frame, whose d axis is aligned with the rotor flux vector. The reference stator voltage is obtained by combining the output signals of the previous controllers, compensated for the d_1-q_1 back-emfs, and expressing the resulting vector in the stationary reference frame α_1-β_1. The rotor flux in the fundamental subspace is estimated by means of a flux observer that integrates the rotor equation, while an incremental encoder measures the mechanical speed.

The control scheme is implemented on a TMS320F28335 development board, produced by Texas Instruments. The switching period is 200 µs. The computational time of the entire control system with a traditional SVPWM technique is equal to 65 µs, while the control system with the modulation strategy in the extended linear modulation region is 96 µs, which corresponds to an increase of 31 µs in the calculation time due to the overmodulation algorithm.

The parameters of the field-oriented vector control and the bandwidth of the control loops are shown in Table IV.

As can be seen, the current vector $\bar{\imath}_3$ is not directly controlled and is free to change, so its behavior does not depend on the control system. Conversely, one could suspect that the current regulators might alter the trajectory of $\bar{\imath}_1$, since
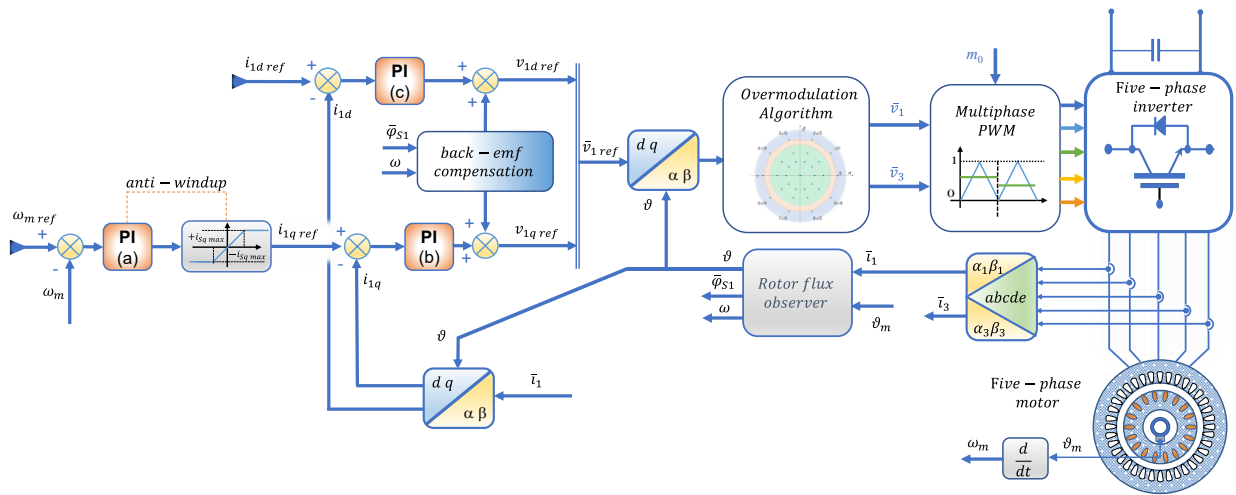
Fig. 7. Block diagram of the rotor field-oriented control scheme for the five-phase induction motor drive used in the experimental tests.

TABLE IV

GAINS AND BANDWIDTHS OF THE REGULATORS

PI (a)	PI (b - c)
Proportional gain K_p=0.28 A/V	Proportional gain K_p=92 A/V
Integral gain K_i=0.7 A/Vs	Integral gain K_i=2000 A/Vs
Bandwidth 2 Hz	Bandwidth 238 Hz

the bandwidth of the current controllers is greater than the frequency of the most significant overmodulation voltage harmonics (3, 7, 9, 11) at the rated speed. However, since the inverter already operates in overmodulation, this compensation action is neither possible nor significant.

B. Extended Linear Modulation

Fig. 8 shows the loci of $\bar{m}_1$ and $\bar{m}_3$ in the extended linear region (0.523 < MI < 0.616). This figure has been obtained by overlapping the results from six different experimental tests. The space vector related to the first harmonic of the magnetic field $\bar{m}_1$ tracks a circular orbit, whereas the path of $\bar{m}_3$ is more complicated and strongly dependent on the value of the modulation index MI. Similar results have already been published by other authors, who based their approach on the SVM technique [18].

In Fig. 9, a motor speed transient is presented. If the motor speed is less than about 100 rpm, the inverter operates in a linear region. After this speed, the use of the space vector $\bar{m}_3$ allows operating in the extended linear modulation region. As already highlighted in (21), λ is a negative quantity, while μ generally assumes zero, negative and positive values.

As soon as the inverter enters into the extended linear modulation region, some modulating signals are forced to zero or to one for long periods, which causes a drastic reduction in the number of inverter commutations and consequently in the switching losses. The drawback is the presence of a distorted phase current, which get worse as the modulation index rises.

Fig. 10 summarizes in a single image the spectrum of the phase current as a function of the modulation index for different modulation strategies. The amplitude of the phase current is normalized by the current present at the boundary of the linear region. The harmonics produced by the space
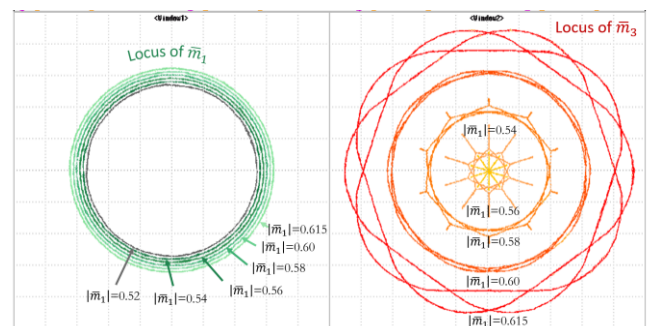

Fig. 8. Loci of space vector $\bar{m}_1$ (20 V/div) and $\bar{m}_3$ (4 V/div) in extended modulation region for different modulation index. (10 V/div).
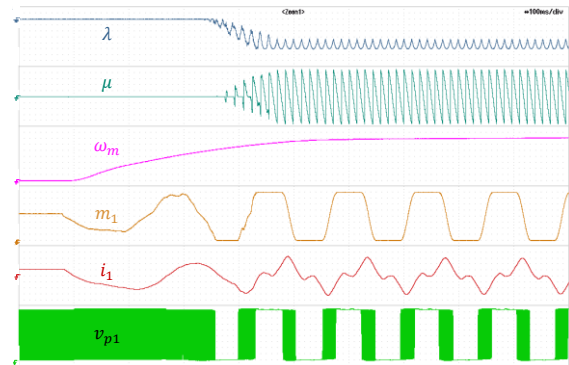

Fig. 9. Speed transient of the motor from 0 to 144 rpm. Waveforms of λ (0.025/div), μ (0.025/div), mechanical speed ω_m (20 rpm/div), modulating signal m_1 of phase 1 (0.125/div), current of phase 1 (2 A/div), and pole voltage v_{p1} of phase 1 (12 V/div).

vector $\bar{v}_1$ and those produced by $\bar{v}_3$ have been plotted with different colors [10].

In the extended linear modulation region, the MD, MPE and Bs techniques are equal, and the first harmonic increases linearly as a function of the modulation index. On the contrary, the fundamental harmonic of SVPWM is not a linear function of the modulation index, as already shown in Fig. 5. However, the use of vector $\bar{v}_3$ generates the presence of the third and seventh harmonic components in the currents. Consequently, the Total Harmonic Distortion (THD) of the
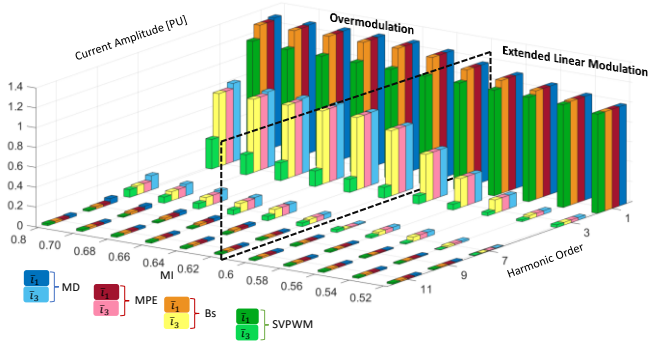
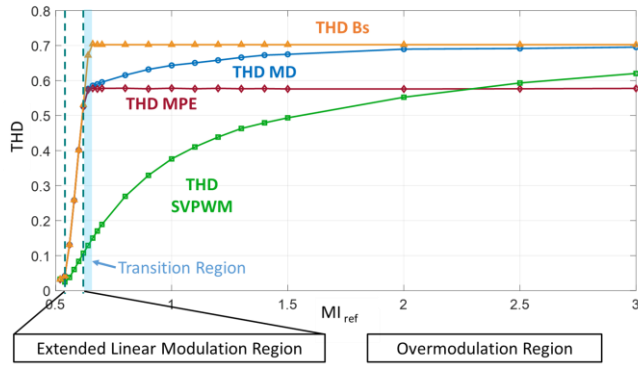Fig. 10. Spectrum of the phase current for different modulation indexes.

Fig. 11. THD of the stator current in different modulation regions as a function of the modulation index.

stator current increases significantly (Fig. 11). The extent of this distortion is strongly dependent on the electrical parameters of the machine, as explained in Section II.E.

C. Overmodulation Region

When the inverter operates in the overmodulation region, the voltage references cannot be followed any longer, so the paths of the reference and actual space vectors cannot be equal. Fig. 12 shows how the paths of the space vectors change in the overmodulation region. Each subfigure has been obtained by overlapping the results from five tests with different values of $\bar{m}_{1,ref}$ and $\bar{m}_{3,ref}$. The three over-modulation strategies presented (MD, MPE and Bs) draw the same trajectories of $\bar{m}_1$ and $\bar{m}_3$ in the complex planes α_1-β_1
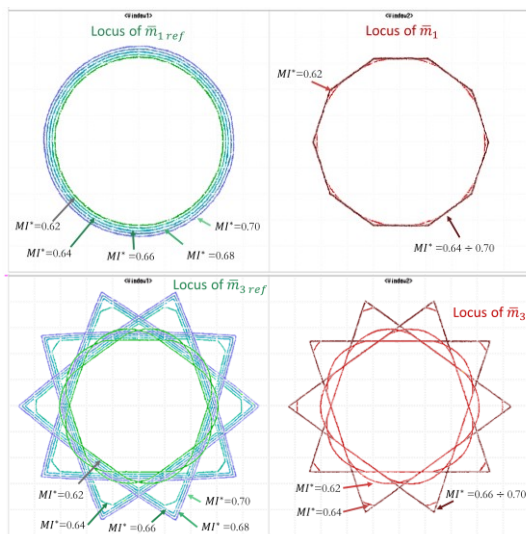

Fig. 12. Loci of $\bar{m}_{1,ref}$ (20 V/div), $\bar{m}_1$ (20 V/div), $\bar{m}_{3,ref}$ (6 V/div), $\bar{m}_3$ (6 V/div) in the overmodulation region with different values of the modulation index when using MD or MPE strategies.
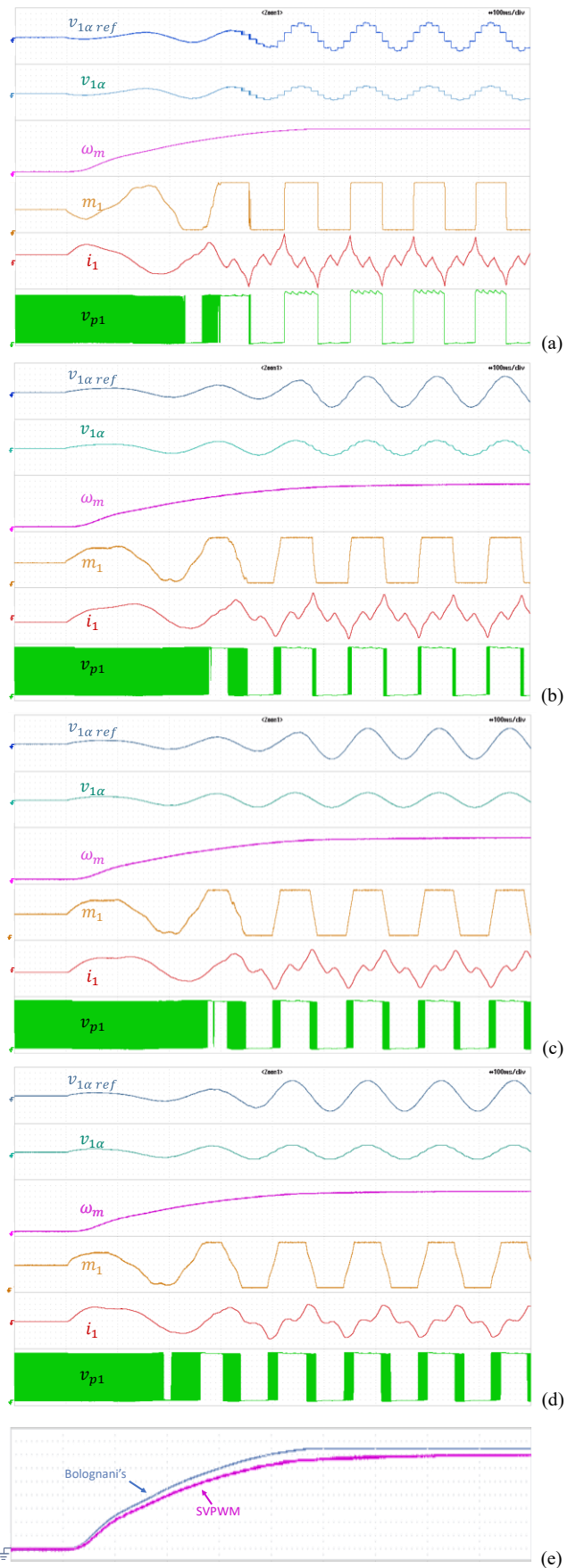
Fig. 13. Speed transients of the motor with different overmodulation strategies. (a) Bolognani's strategy. (b) MD strategy. (c) MPE strategy. (d) SVPWM strategy. (e) Superposition of the speed transients (a) and (d). Waveforms of $v_{1,ref,\alpha}$ (50 V/div), $v_{1\alpha}$ (50 V/div), mechanical speed ω_m (20 rpm/div), modulating signal m_1 of phase 1 (0.125/div), current of phase 1 (2 A/div), and pole voltage v_{p1} of phase 1 (12 V/div).

and α_3-β_3. What differentiates the modulation techniques is the speed with which the path is covered. For all these techniques, the actual space vector $\bar{m}_1$ is constrained within a regular decagon while the reference $\bar{m}_{1,ref}$ continues to follow a circular trajectory. The space vectors $\bar{m}_3$ and $\bar{m}_{3,ref}$ follow a path with the shape of a decagram.

In terms of harmonic distortion of the phase current, the MD, MPE and Bs overmodulation strategies behave differently when the modulation index exceeds 0.616. In particular, the MD technique produces a fundamental harmonic of voltage slightly higher than the MPE technique but worsens the THD of the currents (Fig. 9).

Fig. 12 shows how the SVPWM modulation tends to resemble the MD technique for modulation indexes greater than 2.5, while the MPE technique does not rise any more after reaching the saturation level.

Fig. 13 shows a speed transient of the electric drive operated with different overmodulation strategies. In all tests, the parameters of the control system are unchanged, and the load torque is negligible. The speed setpoint is much greater than the rated speed, so the electric drive reaches the highest speed that is compatible with the available voltage. The modulation index increases up to 1.3, which is adopted as a saturation threshold for the current regulators. As illustrated in Fig. 11, at the end of the transient, the Bs technique shows the highest distortion of the stator current, but it produces the largest magnitude of the vector $\bar{v}_1$, which enables the motor to reach a higher speed (159 rpm). The MPE technique has lower THD, and the final speed (149 rpm) is slightly lower than the one reached by MD technique (156 rpm). Finally, the SVPWM technique has the lowest harmonic content but the machine cannot go beyond 145 rpm.

Fig. 13(e) shows the superposition of the speed transient with Bolognani's overmodulation and SVPWM. As can be seen, not only Bolognani's overmodulation allows the drive to reach a higher speed but also significantly accelerates the speed transient.

All these strategies reduce switching losses, as can be seen from the waveform of the pole voltage v_{p1}. To emphasize this aspect, Fig. 14 compares the average switching frequencies of the four strategies proposed when the motor operates in the rated conditions. In the overmodulation region, the MPE strategy reduces the number of commutations by about 80% while the MD and SVPWM techniques tend to the square
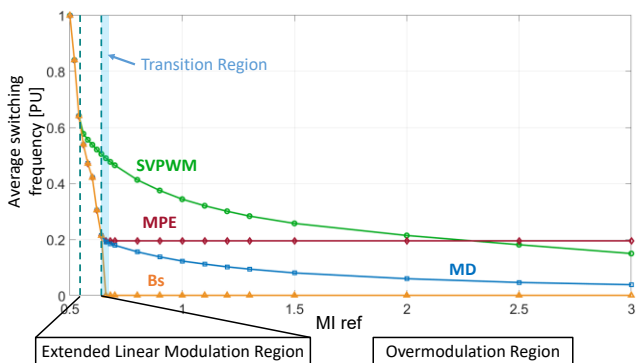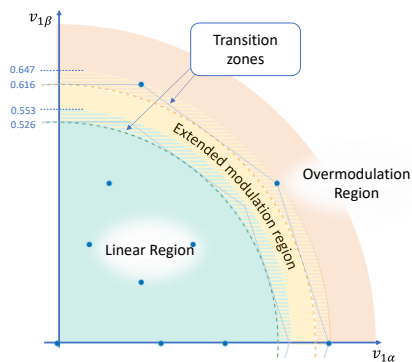

Fig. 15. Detail of the modulation regions in a five-phase inverter to highlight the transition zones.
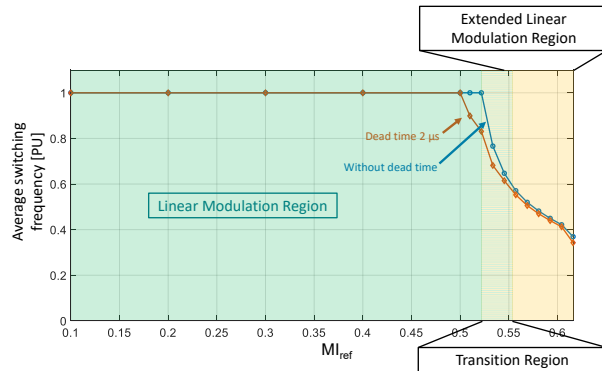

Fig. 16. Switching frequency for MD, MPE and Bolognani's strategies as a function of the modulation index to highlight the effect of the dead time.

wave operation without reaching it. Conversely, the Bolognani's overmodulation strategy quickly reaches the square wave operation.

There are two phenomena that reduce the number of commutations during the transition between the linear and extended linear region. The first phenomenon depends on the inverter dead time. The effect of dead time in a multiphase inverter is similar to one in a standard three-phase inverter. The dead time distorts the voltage produced by the inverter according to the sign of the phase current and reduces the number of commutations when the modulating signal is close to zero or one. The techniques that compensate the effect of the dead time improve the quality of the current waveform, but they do not avoid cancelling some commutations when the modulating signals are near to the boundaries (0 or 1).

The second phenomenon is the presence of "transition zones" between the modulation regions. They are illustrated in Fig. 15, which shows a detail of Fig. 2. Between the linear and the extended linear region and between the extended linear and the overmodulation region there are two transition zones. In steady state condition, the space vector $\bar{v}_{1,ref}$ describes a circular trajectory in complex plane $v_{1\alpha}$-$v_{1\beta}$. When the magnitude of $\bar{m}_1$ is between 0.526 and 0.553, the inverter operates alternately in a linear or extended linear region depending on the phase angle of the vector $\bar{m}_1$. A similar phenomenon happens also when the amplitude of $\bar{m}_1$ is between 0.616 and 0.647. During these transition phases, the number of commutations drops rapidly.

The effect of the dead time and the presence of transition zones reduce the number of switch commutations. Fig. 16

Fig. 14. Average switching frequency of SVPWM, MD, MDE and Bolognani's strategies for different values of the modulation index.

shows a comparison between the experimental results of the inverter with the rated dead time (2 μs) and the numerical simulations when the dead time is ideally zero. The dead time reduces the number of switch commutations even before leaving the linear region, while the number of commutations drops sharply in the transition region. Finally, in the extended linear region, the effect of the dead time is marginal.

IV. CONCLUSION

The electric drives that use an inverter operating into the overmodulation region to obtain a boost in the dynamic performance of the motor are now widespread. The main contribution of this paper is to present a coherent analysis of the problem of overmodulation in five-phase inverters and to extend some well-known three-phase overmodulation methods to five-phase systems. It has been shown that, in multiphase inverters, it is possible to define a new region, different from linear and overmodulation regions, in which it is possible to reach higher values of the modulation index as long as a certain level of voltage distortion is acceptable. Although many papers investigating the problem of overmodulation are based on SVM, which seems to provide an intuitive representation of the problem, the analysis developed in this paper is entirely focused on carrier-based PWM and leads to a closed-form expression of the modulating signals in the extended linear region. This solution allows extending the linear range of the converter by 17%.

If the reference voltage is outside the linear and extended-linear operating regions, it is still possible to extend further the output voltage by 3-4% if one accepts the voltage distortion of the overmodulation operation. Also, different overmodulation strategies are possible. The performance of some strategies, which have been derived from the corresponding overmodulation techniques for three-phase inverters, has been compared experimentally, through steady-state and transient tests.

APPENDIX A

Let us verify that (32)-(34) leads to the generation of the voltage vector $\bar{v}_1$ having the minimum distance from the desired vector $\bar{v}_{1,ref}$. By definition, $\bar{m}_{1,ref}$ and $\bar{m}_1$ are as follows:

$$\bar{m}_1 = \frac{2}{5}(m_H \ \bar{\alpha}_H + m_U \ \bar{\alpha}_U + m_M \ \bar{\alpha}_M + m_D \ \bar{\alpha}_D \\ + m_L \ \bar{\alpha}_L) \tag{A1}$$

$$\bar{m}_{1,ref} = \frac{2}{5}(m_{H,ref} \ \bar{\alpha}_H + m_{U,ref} \ \bar{\alpha}_U + m_{M,ref} \ \bar{\alpha}_M \\ + m_{D,ref} \ \bar{\alpha}_D + m_{L,ref} \bar{\alpha}_L). \tag{A2}$$

In the overmodulation region, $\bar{m}_{3,ref}$ is chosen according to (28). Consequently, (27) ensures that $m_{H,ref}$ is equal to $m_{U,ref}$, and $m_{L,ref}$ is equal to $m_{D,ref}$. Also, $m_{H,ref}$ must be greater than one, while $m_{L,ref}$ must be lower than zero. Therefore, m_H and m_U are clamped to 1, while m_D and m_L are clamped to 0. The only modulating signal in the range [0,1] is $m_{M,ref}$, which coincides with m_M. Then, (A1) and (A2) can be rewritten as follows:

$$\bar{m}_1 = \frac{2}{5}(\bar{\alpha}_H + \bar{\alpha}_U + m_{M,ref} \ \bar{\alpha}_M). \tag{A3}$$

$$\bar{m}_{1,ref} = \frac{2}{5}(m_{H,ref} \ \bar{\alpha}_H + m_{H,ref} \ \bar{\alpha}_U + m_{M,ref} \ \bar{\alpha}_M \\ + m_{L,ref} \ \bar{\alpha}_D + m_{L,ref} \ \bar{\alpha}_L). \tag{A4}$$

The voltage error is

$$\overline{\Delta m}_1 = \bar{m}_{1,ref} - \bar{m}_1 = \\ \frac{2}{5}[(m_{H,ref} - 1)(\bar{\alpha}_H + \bar{\alpha}_U) + m_{L,ref}(\bar{\alpha}_D + \bar{\alpha}_L)]. \tag{A5}$$

The voltage error is the smallest when $\overline{\Delta m}_1$ is orthogonal to the boundary of the overmodulation region. This condition can be written as follows:

$$\overline{\Delta m}_1 \cdot (\bar{\alpha}_H + \bar{\alpha}_L) = 0 \tag{A6}$$

where $\bar{\alpha}_H + \bar{\alpha}_L$ is the direction of the side of the generic decagon sector (Fig. 4). Since it can be shown that

$$(\bar{\alpha}_H + \bar{\alpha}_U) \cdot (\bar{\alpha}_H + \bar{\alpha}_L) = (\bar{\alpha}_D + \bar{\alpha}_L) \cdot (\bar{\alpha}_H + \bar{\alpha}_L) \tag{A7}$$

equation (A6) becomes

$$[m_{H,ref} + m_{L,ref} - 1](\bar{\alpha}_H + \bar{\alpha}_U) \cdot (\bar{\alpha}_H + \bar{\alpha}_L) = 0. \tag{A8}$$

Replacing (34) in (A8) leads to the expression (32) of the zero-sequence component.

As far as (A7) is concerned, it can be easily verified that it can be rewritten in the following simpler form:

$$(\bar{\alpha}_U - \bar{\alpha}_D) \cdot (\bar{\alpha}_H + \bar{\alpha}_L) = 0 \tag{A9}$$

where

$$\bar{\alpha}_U - \bar{\alpha}_D = 2j \sin\left(\pi \frac{U - D}{5}\right) e^{j\frac{\pi}{5}(U+D-2)} \tag{A10}$$

$$\bar{\alpha}_H + \bar{\alpha}_L = 2 \cos\left(\pi \frac{H - L}{5}\right) e^{j\frac{\pi}{5}(H+L-2)}. \tag{A11}$$

The last step of the proof requires noting that, with the usual values of $\bar{m}_3$, the ordering of the modulating signals is so that $H + L - U - D = 5n$, with $n \in \mathbb{Z}$. This condition and (A10)-(A11) ensure that (A9) is true.

REFERENCES

[1] L. de Lillo, L. Empringham, P. W. Wheeler, S. Khwan-On, C. Gerada, M. N. Othman, X. Huang, "Multiphase power converter drive for fault-tolerant machine development in aerospace applications," IEEE Trans. Ind. Electron., vol. 57, no. 2, pp. 575-583, Feb. 2010.

[2] R. Bojoi, A. Cavagnino, A. Tenconi, S. Vaschetto, "Control of shaft-line-embedded multiphase starter/generator for aero-engine," IEEE Trans. Ind. Electron., vol. 63, no. 1, pp. 641-652, Jan. 2016.

[3] G. Sulligoi, A. Tessarolo, V. Benucci, A. M. Trapani, M. Baret, F. Luise, "Shipboard power generation: design and development of a medium-voltage dc generation system," IEEE Ind. Appl. Magazine, vol. 19, no. 4, pp. 47-55, July-Aug. 2013.

[4] Jingya Dai, Sang Woo Nam, M. Pande, G. Esmaeili, "Medium-voltage current source converter drives for marine propulsion system using a dual-winding synchronous machine," IEEE Trans. on Ind. Appl., vol. 50, no. 6, pp. 3971-3976, Nov.-Dec. 2014.

[5] M. Mengoni, L. Zarri, A. Tani, L. Parsa, G. Serra, D. Casadei, "High-torque-density control of multiphase induction motor drives operating over a wide speed range," IEEE Trans. Ind. Electron., vol. 62, no. 2, pp. 814-825, Feb. 2015.

[6] L. Li, K. Lee, K. Bai, X. Ouyang, H. Yang, "Inverse models and harmonics compensation for suppressing torque ripples of multiphase

permanent magnet motor," IEEE Trans. Ind. Electron., vol. 65, no. 11, pp. 8730 - 8739, Feb. 2018.

[7] W. Kong, M. Kang, D. Li, R. Qu, D. Jiang, C. Gan, "Investigation of spatial harmonic magnetic field coupling effect on torque ripple for multiphase induction motor under open fault condition," IEEE Trans. Pow. Electron., vol. 33, no. 7, pp. 6060 - 6071, Aug. 2017.

[8] E. Levi, M. Jones, S.N. Vukosavic, H.A. Toliyat, "A novel concept of a multiphase, multimotor vector controlled drive system supplied from a single voltage source inverter," IEEE Trans. Pow. Electron., vol. 19, no. 2, pp. 320 - 335, Mar. 2004.

[9] E. Levi, M. Jones, S.N. Vukosavic, H.A. Toliyat, "Operating principles of a novel multiphase multimotor vector-controlled drive," IEEE Trans. Energ. Convers., vol. 19, no. 3, pp. 508 - 517, Aug. 2004.

[10] J. M., O. López, A. G. Yepes, A. Vidal, F. D. Freijedo, P. Fernández-Comesaña, J. Gandoy, "Graphical diagram for subspace and sequence identification of time harmonics in symmetrical multiphase machines," IEEE Trans. Ind. Electron., vol. 61, no. 1, pp. 29 - 42, Jen. 2013.

[11] E. Levi, D. Dujic, M. Jones, G. Grandi, "Analytical determination of dc-bus utilization limits in multiphase VSI supplied AC drives," IEEE Trans. Energy Conv., vol. 23, no. 2, pp. 433-443, June 2008.

[12] Y. Kwon, S. Kim, S. Sul, "Six-step operation of PMSM with instantaneous current control," IEEE Trans. Ind. Electron., vol. 50, no. 4, pp. 2614 - 2625, Apr. 2014.

[13] X. Zhang, G. Foo, "Overmodulation of constant-switching-frequency-based DTC for reluctance synchronous motors incorporating field-weakening operation," IEEE Trans. Ind. Electron., vol. 66, no. 1, pp. 37 - 47, Jan. 2019.

[14] P. Stumpf, S. Halàsz, "Optimization of PWM for the overmodulation region of two-level inverters," IEEE Trans. Ind. Appl., vol. 54, no. 4, pp. 3393 - 3404, Jul. 2018.

[15] C. Zhou, G. Yang, J. Su, "PWM strategy with minimum harmonic distortion for dual three-phase permanent-magnet synchronous motor drives operating in the overmodulation region," IEEE Trans. Pow. Electron., vol. 31, no. 2, pp. 1367 - 1380, Feb. 2016.

[16] T. Komrska, T. Glasberger, Z. Peroutka, "Universal PWM modulator for multiphase drives with a minimum infinity-norm approach," IEEE Trans. Ind. Electron., vol. 63, no. 10, pp. 5979 - 5987, Oct. 2016.

[17] M. J. Duran, F. Barrero, J. Prieto, "DC-bus utilization and overmodulation performance of five-phase voltage source inverters using model predictive control," in Proc. IEEE International Conference on Industrial Technology (ICIT), Vian del Mar, Chile, 2010.

[18] G. Carrasco, A. Silva, "Space Vector PWM method for five-phase two-level VSI with minimum harmonic injection in the overmodulation region," IEEE Trans. Ind. Electron., vol. 60, no. 5, pp. 2042 - 2053, May 2013.

[19] M. Priestley, J. E. Fletcher, "Space-Vector PWM Technique for Five-Phase Open-End Winding PMSM Drive Operating in the Overmodulation Region," IEEE Trans. Ind. Electron., vol. 65, no. 9, pp. 6816 - 6827, Sept. 2018.

[20] J. Prieto, F. Barrero, M. Duran, S. Marín, M. Perales, "SVM procedure for n-phase vsi with low harmonic distortion in the overmodulation region," IEEE Trans. Ind. Electron., vol. 61, no. 1, pp. 92 -97, Jan. 2014.

[21] T. Komrska, T. Glasberger, Z. Peroutka, "Carrier-based PWM with minimum infinity norm for overmodulation area of five-phase converters," in Proc. 18th European Conference on Power Electronics and Applications (EPE'16 ECCE Europe), Karlsruhe, Germany, 2010.

[22] A. G. Yepes, J. Doval-Gandoy, H. A. Toliyat, "Improvement in DC-link utilization with reduced current and torque deterioration for five-phase drives by combination of circulating-current filters and simple carrier-based PWM based on closed-form expressions," IEEE Trans. Ind. Electron.. Early preview.

[23] S. Karugaba, O. Ojo, "A Carrier-Based pwm modulation technique for balanced and unbalanced reference voltages in multiphase voltage-source inverters," IEEE Trans. Ind. Appl., vol. 48, no. 6, pp. 2102-2109, Nov. 2012.

[24] L. Zarri, M. Mengoni, A. Tani, G. Serra, D. Casadei, "Minimization of the power losses in IGBT multiphase inverters with carrier-based pulsewidth modulation," IEEE Trans. Ind. Electron., vol. 57, no. 11, pp. 3695 - 3706, Feb. 2010.

[25] D. Dujic, M. Jones, E. Levi, "Analysis of output current ripple rms in multiphase drives using space vector approach," IEEE Trans. Pow. Electron., vol. 24, no. 8, pp. 1926 - 1938, Aug. 2009.

[26] D. Dujic, M. Jones, E. Levi, "Analysis of output current-ripple rms in multiphase drives using polygon approach," IEEE Trans. Pow. Electron., vol. 25, no. 7, pp. 1838 - 1849, Jul. 2010.

[27] Z. Nie, N. Schofield, "Multi-phase VSI DC-link capacitor considerations," IET Pow. Appl., vol. 13, no. 3, pp. 1838 - 1849, Mar. 2019.

[28] A. Yepes, J. Malvar, A. Vidal, O. Lopez, J. Gandoy, "Current harmonics compensation based on multiresonant control in synchronous frames for symmetrical n-phase machines," IEEE Trans. Ind. Electron., vol. 62, no. 5, pp. 2708 - 2720, May 2015.

[29] M. Mengoni, L. Zarri, A. Tani, G. Serra, D. Casadei, "Injection of third-order spatial field harmonics for sensorless speed estimation in multiphase induction motor drives," Proc. of IEEE International Symposium on Sensorless Control for Electrical Drives (SLED), Catania, Italy 2017.

[30] A. Tani, M. Mengoni, L. Zarri, G. Serra, D. Casadei, "Control of multiphase induction motors with an odd number of phases under open-circuit phase faults," IEEE Trans. Pow. Electron., vol. 27, no. 2, pp. 565 - 577, Feb. 2012.

[31] A. Yepes, J. Riveros, J. Gandoy, F. Barrero, O. Lopez, B. Bogado, M. Jones, E. Levi, "Parameter identification of multiphase induction machines with distributed windings—part 1: sinusoidal excitation methods," IEEE Trans. on Ener. Conv., vol. 27, no. 4, pp. 1056 - 1066, Dec. 2012.

[32] X. Guo, M. He, Y. Yang, "Over modulation strategy of power converters: a review," IEEE Access, vol. 6, pp. 69528 - 69544, Oct. 2018.

[33] S. Bolognani, M. Zigliotto, "Novel digital continuous control of SVM inverters in the overmodulation range," IEEE Trans. Ind. Appl., vol. 33, no. 2, pp. 525–530, Mar./Apr. 1.

[34] A. Iqbal, S. Moinuddin, "Comprehensive relationship between carrier-based PWM and space vector PWM in a five-phase VSI," IEEE Trans. Pow. Electron., vol. 24, no. 10, pp. 2379-2390, Oct. 2009.

Luca Vancini received the M.Sc. degree in Electrical Engineering in 2018 from the University of Bologna, Bologna, Italy. Currently he is pursuing a PhD in electrical engineering with the Department of Electric, Electronic and Information Engineering "G. Marconi", University of Bologna. His research interests include power electronics, control of multiphase converters and diagnostic techniques for multiphase machines.

Michele Mengoni was born in Forlì, Italy. He received the M. Sc. and Ph. D. degrees in Electrical Engineering from the University of Bologna, Bologna, Italy, in 2006 and 2010, respectively. He is currently a Senior Assistant Professor with the Department of Electric, Electronic and Information Engineering "G. Marconi", University of Bologna. His research interests include design, analysis, and control of three phase electric machines, multiphase drives, and ac/ac matrix converters.
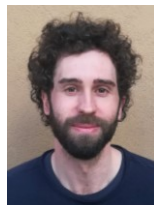
Gabriele Rizzoli received the M.Sc and Ph.D. degree in Electrical Engineering, respectively in 2012 and 2016, from the University of Bologna, Bologna, Italy. In 2015 he was a visiting student at Virginiatech (CPES), Blacksburg, Virginia, United States of America. He is currently an assistant professor with the Department of Electrical, Electronic and Information Engineering "G. Marconi" of the University of Bologna. His research interests include the design of electrical machines, the development and control of high-efficient power converters for automotive and renewable energy applications.

Giacomo Sala (M'20) received the B. Sc. in Power Engineering in 2012 from the University of Bologna, Bologna, Italy, the M. Sc. degree and the Ph. D. degree in Electrical Engineering, respectively in 2014 and 2018, from the same university. He was a research assistant at The University of Nottingham, UK, from 2018 to 2019. In 2019, he joined the Dept. of Electrical Engineering "G. Marconi" of the University of Bologna, where he is currently an assistant professor. His research interests include design, modelling and control of multiphase electrical machines, fault tolerant controls and fault diagnosis of electric drives.

Luca Zarri (M'05-SM'12) received the M. Sc. and Ph.D. degree in Electrical Engineering from the University of Bologna, Bologna, Italy, in 1998 and 2007, respectively. Currently, he is a Full Professor of power electronics, electrical machines and drives with the Department of Electrical, Electronic, and Information Engineering "Guglielmo Marconi", University of Bologna. He has authored or coauthored more than 150 scientific papers. His research activity concerns the control of power converters and electric drives. He is a senior member of the IEEE Industry Applications, IEEE Power Electronics and IEEE Industrial Electronics Societies.

Angelo Tani received the M. Sc. degree in Electrical Engineering, with honors, from the University of Bologna, Bologna, Italy, in 1988. Currently he is a Full Professor of power electronics, electrical machines and drives with the Department of Electrical, Electronic and Information Engineering "Guglielmo Marconi", University of Bologna. He has authored more than 200 papers published in technical journals and conference proceedings. His current activities include modelling, control and fault diagnosis of multiphase electric machines.